Application of Two-Phase Immersion Cooling Technique for Performance Improvement of High Power and High Repetition Avalanche Transistorized Subnanosecond Pulse Generators

Yanan Wang, *Member, IEEE*, Linyuan Ren, Zihao Yang, Zichen Deng, and Weidong Ding, *Member, IEEE*

***Abstract*—In this article, we show the feasibility of improving the performance of a high voltage and high repetition avalanche transistor pulse generator by applying a two-phase immersion cooling technique. The forced air cooling, single-phase immersion cooling, and two-phase immersion cooling techniques were applied to a 60-stage subnanosecond pulse generator. The experimental results indicate that the two-phase immersion cooling technique can effectively control the temperature rising of the avalanche transistor and, thus, reduce the time base jitter and voltage amplitude jitter. Five types of dielectric fluid with different boiling temperatures were comparatively studied. The FC-72 was finally adopted for the balanced performance on voltage amplitude and repetition rate. The two-phase immersion cooling technique could reduce the thermal resistance between the case and ambient and increase the maximum power from 330 to 876 mW. With this cooling method, the surface temperature of the transistor can be effectively controlled below 62 °C. The pulse generator could achieve outstanding performance with a voltage of 2350 V and a rise time of 180 ps. It can work stably at 200 kHz for more than 30 min, and the burst repetition rate could be 260 kHz within 1 min. This article offers new perspectives in the design of high repetitive avalanche transistorized subnanosecond generators.**

***Index Terms*—Avalanche transistors, high repetition rate, long-term reliability, sub-nanosecond pulse generator, two-phase immersion cooling.**

I. Introduction

WITH the merits of fast switching speed (>100 V/ns), moderate applying voltage, versatile turn-on method, bipolar transistors with avalanche operation mode are extensively utilized in the nanosecond and subnanosecond pulse generators. The high voltage, high repetitive nanosecond, and sub-nanosecond pulses utilizing avalanche transistors are attracting substantial attention in numerous industrial applications, such as pumping electro-optically lasers [1], sustaining pulsed electric field for the medical irreversible electroporation [2], driving different types of discharge plasmas in amounts of fields [3], the chemical analysis of minute materials, developing electromagnetic interference environment for security defence and ground-penetrating radar [4]. It is always required that the output pulses have sufficient high amplitude, a fast-rising time, high repetition rate, high stability, and reliability. These properties bring a great challenge for the design and construction of such pulse generators.

With the worldwide researchers' efforts, the performance of avalanche transistor pulse generators has been greatly improved. Different topologies have been developed to increase the output voltage and current amplitude, including Marx bank circuit (MBC) [5]–[8], direct pulse adding (DPA) [9], MBC with microstrip line [10], [11], MBC with transmission line transformer (TLT) [9], [12], linear transformer driver (LTD) [13]. Fig. 1 shows the recent advances of avalanche transistorized pulse generators and the typical application in driving atmospheric pressure plasma jet and developing ultra-wideband radiation system [14]. However, the main trouble with these types of pulse generators is the avalanche transistor's operation mode: a transistor in the chain can suddenly shorten, which will not cause the damage immediately but the degradation. In addition, the output performance is limited by heat transfer, and the reliability is also closely dependent on the semiconductor device's features: the maximum temperature and the temperature gradients and fluctuations [15], [16]. Jiang [17], [18] pointed out that thermal management is an important factor that needs to be considered in high repetitive pulse power systems. The thermal problem could be more severe in a high repetition rate [19]. When operating with high frequency, the higher power dissipation and the heat accumulation could lead to a huge temperature rising in ambient. According to the datasheet of the avalanche transistor, the rated maximum power dissipation is 330 mW while it drops by 2.64 mW with an ambient temperature rising by 1 °C [20]. Moreover, the pulse drift and jitter will also increase with the temperature rising, which causes severe degradation of the output

Manuscript received April 8, 2021; revised July 19, 2021; accepted September 5, 2021. Date of publication September 9, 2021; date of current version November 30, 2021. This work was supported in part by National Natural Science Foundation of China under Grant No. 52007147, in part by China Postdoctoral Science Foundation under Grant No. 2020M683480, and in part by National Key Laboratory on Electromagnetic Environment Effects under Grant No. 6142205200202. Recommended for publication by Associate Editor J. Popovic-Gerber. *(Corresponding authors: Yanan Wang and Weidong Ding.)*

The authors are with the State Key Laboratory of Electrical Insulation and Power Equipment, School of Electrical Engineering, Xi'an Jiaotong University, Xi'an 710049, China (e-mail: yn.wang_ee@xjtu.edu.cn; 942952182@qq.com; 1399226789@qq.com; 3521976873@qq.com; wdding@xjtu.edu.cn).

Color versions of one or more figures in this article are available at https://doi.org/10.1109/TPEL.2021.3111348.

Digital Object Identifier 10.1109/TPEL.2021.3111348

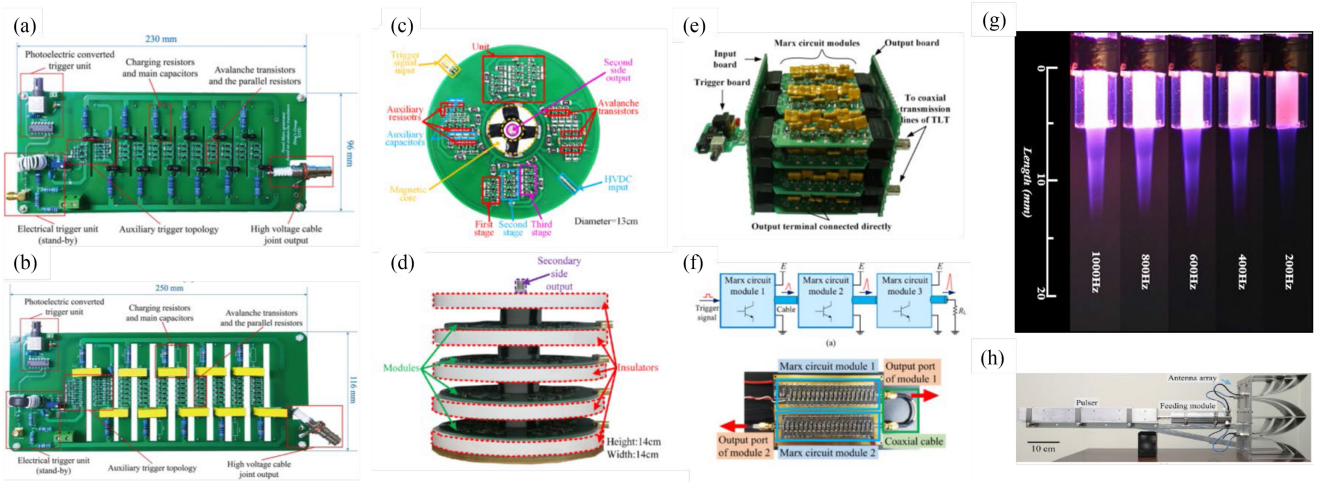

Fig. 1. Recent advances in avalanche transistor pulse generators and their applications. (a) and (b) High-power nanosecond pulse generators with auxiliary triggering topology for the application of gas switch triggering and driving discharge plasma. Marx bank circuit with 3 × 12 stages, 36 avalanche transistors applied in (a) and 6 × 10 stages, 60 avalanche transistors applied in (b) [5]. (c) and (d) High voltage nanosecond pulse generator based on avalanche transistor MBC and LTD, 144 avalanche transistors were utilized [13]. (e) Hybrid pulse combining topology utilizing the combination of MBC, DPA, and TLT [9]. (f) Traveling-wave MBC modules in series connection [14]. (g) Repetitive avalanche transistor pulse generator driving atmospheric pressure plasma jet [7]. (h) Pulse generator utilized to develop ultra-wideband radiation environment simulation [11].

performance. Although heat dissipation and thermal design are the key factors influencing the reliability and durability of avalanche transistor circuits, not enough attention has been paid to the thermal design.

In recent years, cooling technologies have grown significantly to manage higher density heat fluxes in electronics systems such as insulated-gate bipolar transistor (IGBT) power modules and high-performance converters [21], [22]. However, compared with the common electronics system, the avalanche transistors based pulsed power source has special features which post a great challenge to heat management.

1) *Transistor package:* SOT-23 packages are commonly used in avalanche transistors. The reduction in size and weight are their proclaimed advantage, and the lower lead inductance also makes them competitive in switching speed. Nevertheless, due to their low thermal mass, SOT thermal resistance specifications are highly dependent on local environmental conditions. According to Mohamed *et al.* [23], the external thermal resistance is about two-third of the total thermal resistance and thus determines the package's thermal behavior. It implies that great care must be taken in thermal designs. Because of the extremely small surface, direct heat conduction cooling techniques, such as heat sinks, cold plates, and more advanced cooling vapor chamber, are impractical to be implemented on the component.
2) *Relatively high components density and heat flux density:* In order to reduce the rising time of the output pulse, circuit inductance is always minimized, and a compact layout design of the printed circuit board (PCB) circuit is adopted. In avalanche transistorized pulse generators, as shown in Fig. 1, multiple avalanche transistors (up to tens or hundreds of) are serially and parallelly connected and the charging resistors and other components. As a result, the compact design and relatively high component density lead to increased heat flux density. The conventional forced air cooling (FAC) has been applied in some low-frequency applications [9], while it cannot satisfy the high repetition rate condition for its low heat flux (tens of W/cm^2). The liquid immersion cooling technique can deal with the system with high heat dissipation densities. While the corrosion, long-term compacity, and leakage must be considered and tested. The other cooling method, such as jet impingement and spray cooling, which can achieve a very high heat transfer coefficient, is limited by complex cooling flow redistribution, cooling loop leakage, and channel blockage.
3) *Inhomogeneous temperature distribution of different components:* Due to the different operation conditions, transistors' heat dissipation and temperature distribution differ from each other. The inhomogeneous temperature distribution of the avalanche transistor circuit is theoretically analyzed and experimentally observed [14], [24]. Effective cooling is a challenge in transistor devices with concentrated power.
4) *Ultrafast transient process and heat accumulation under high repetition rate:* The temperature in the "hot spot" of the avalanche transistor could reach several hundred kelvins within a single switching process in the nanosecond range and cool down to room temperature after several microseconds without destruction. However, the increasing repetition rate will reduce the time interval between the pulses, and the temperature will finally rise to a certain thermal destruction threshold. The temperature rising process can be fast in a high repetition rate; hence, the cooling technique with fast time response is required.

These features introduce huge challenges to the heat dissipation design. Nevertheless, nearly all publications devoted to avalanche transistor circuits have concentrated on the better means of selecting commercial components, reducing parasitic

inductance and other forms of routine, but the effective heat management method. The overheated transistors impede the stability of pulse generator operation capacity, as well as the output performance. Thus, an effective cooling technique is necessary for the high repetitive pulse generator to control the avalanche transistors temperature and realize the long-term operation stability.

This article proposes utilizing a two-phase change immersion cooling (TPIC) technique to improve a high-power high repetitive avalanche transistor pulse generator. In order to verify the importance of heat management for pulse generators, the power dissipation and temperature rising processes at a high repetition rate are quantitively analyzed. The FAC, single-phase immersion cooling (SPIC), and TPIC techniques have been applied to the pulse generator and studied comparatively. We showed that a great improvement could be achieved with an effective two-phase immersion cooling method applied. Moreover, the different coolants (3M Novec 7000, Novec 7100, Novec 7200, Novec 7300, Novec 7500, FC-72) were thoroughly investigated in TPIC. The characteristics, capabilities, and limitations of these coolants were discussed. Considering the temperature controlling and output parameters of the pulse generator, a selection criterion of coolant for avalanche transistor circuit application is proposed.

The rest of this article is organized as follows. Section II illustrates the topology and structure of the pulse generator and the experimental platform. In Section III, the heat dissipation and temperature rising process are qualitatively analyzed, and the temperature characteristics under different cooling methods are studied. The temperature-rising characteristics with different coolants have been compared. In Section IV, the phase change process of the TPIC is discussed. Moreover, the heat resistances under different cooling techniques have been calculated. Finally, Section V concludes this article.

II. Experimental Characterization

A. Circuit Design of High-Frequency High-Power Marx Generator With Avalanche Transistors

Fig. 2(a) depicts the schematic of the tested subnanosecond pulse generator with avalanche transistors. In order to generate high repetition rate pulses, the parallel charging Marx circuit topology, proposed by Carl E. Baum, is utilized. In this circuit, the isolation charging resistor is connected parallelly, and the charging time of the main capacitor in each stage is almost the same. The advantage of this type of Marx circuit is the fast charging time, while the isolation characteristic is slightly worse compared with the traditional Marx circuit topology with the same resistors. Several elements can be figured in Fig. 2(b) and (c), including avalanche transistors (Diodes, FMMT 417), capacitors (100 pF/1206), and charging resistors. The compact design is adopted to achieve a fast-rising time of the output pulse. And the length of the connection wire between the switches and capacitors is minimized to reduce the overall inductance.

Moreover, the main capacitors with 100 pF are selected, which contributes to the subnanosecond pulse formation [10].

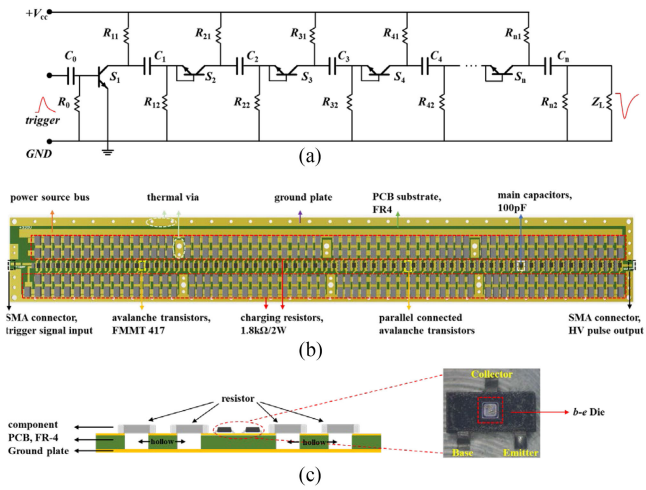

Fig. 2. Schematic of the subnanosecond transistorized Marx generator. (a) Schematic of circuit topology. (b) Top view of the PCB circuit and key components. (c) Side view of the PCB circuit and the photo of the package removed avalanche transistor.

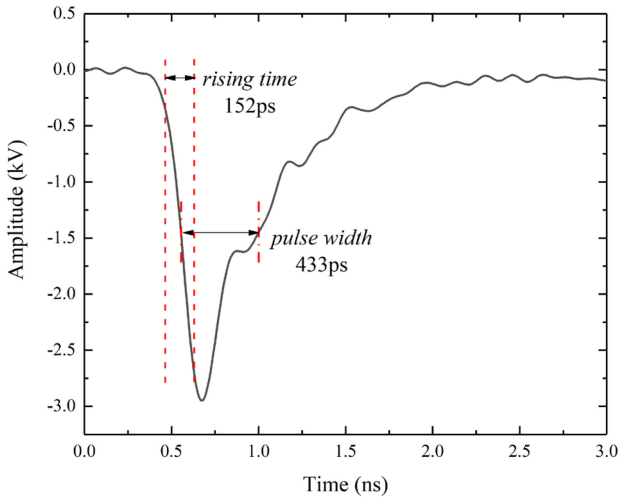

Fig. 3. Typical output waveform of the 60-stage avalanche transistorized subnanosecond pulse generator.

A 60-stage Marx circuit is developed with the serial connection of avalanche transistors and main capacitors to achieve high amplitude output. In addition, a ground plate is arranged on the bottom layer of the PCB to form a transmission line structure, and the width of the switches and capacitors' solder plate is calculated and design to realize an optimal impedance match to minimize the traveling wave reflection. Fig. 3 shows the typical output waveform of the avalanche transistor-based pulse generator. The output voltage amplitude is 2950 V on a 50 Ω load impedance, and the rising time is about 152 ps at a frequency of 1 Hz.

The maximum repetition rate of the pulse generator mainly depends on two aspects: (1) the charging time of the main capacitors; (2) the heat dissipation capacity of the components. The charging time is almost 3 to 6 times the time constant of the charging circuit $\tau = RC$ (R represents the total resistance of the charging resistors, and C is capacitance in each stage).

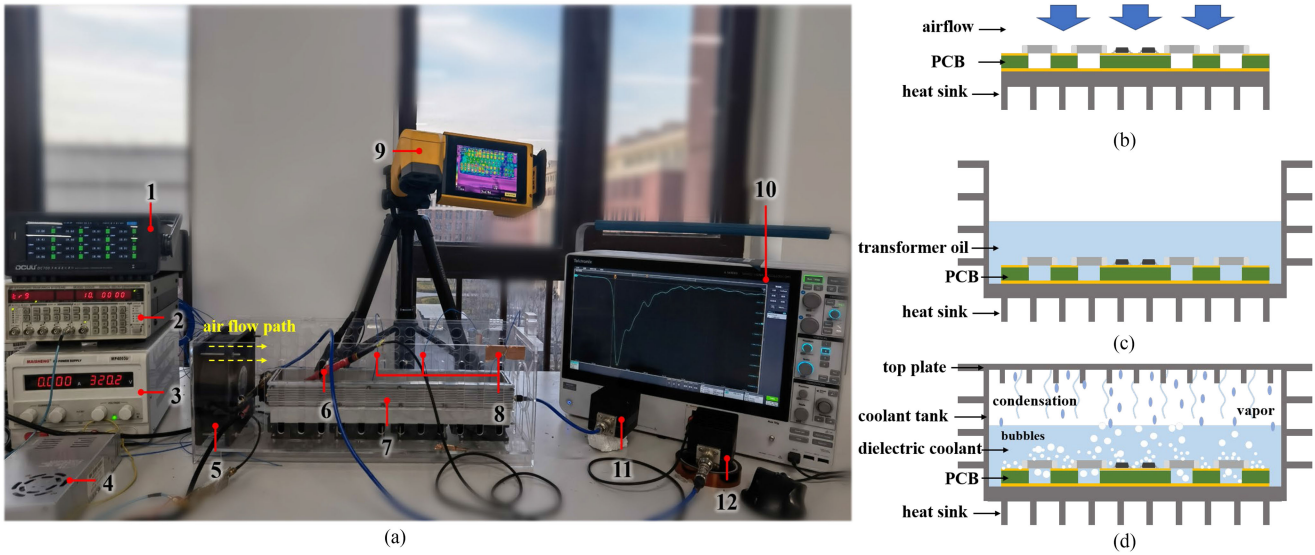

Fig. 4. (a) Photograph of the experimental setup showing the: (1) multichannel thermocouple recorder, (2) trigger signal generator (Stanford Instrument, DG 645), (3) dc power source (400 V, 3 A) to supply pulse generator, (4) dc power source to supply the trigger generator (110 V, 2 A), (5) fan for the vessel cooling in SPIC and TPIC (12 m^3/min), (6) high-voltage probe to measure U_c during switch operation, (7) high-frequency avalanche transistor pulse generator with aluminum vessel, (8) thermocouple sensors, (9) infrared thermal imager (Fluke TiX 501), (10) oscilloscope to record output voltage waveform (Tektronix 6 series, 6 GHz, 25 Gs/S), (11) and (12) attenuators to attenuate high voltage pulse (DC-4 GHz, 50 dB). (b) Schematic of FAC, (c) schematic of SPIC (cooling fan not shown), and (d) schematic of two-phase immersion cooling (cooling fan not shown).

The charging time needs to be sufficiently short to guarantee that the main capacitors could finish recharging before the next shot when operating at a high repetition rate. Nevertheless, the resistance of the charging resistor also needs to be large enough to isolate subnanosecond pulse from the ground and dc source to achieve high output amplitude. Considering the tradeoff between the two requirements, we adopted the resistance $R = 7.2$ kΩ. Furthermore, the charging time constant is approximately 7.2×10^{-7} s. Thus, the maximum theoretical frequency of the circuit is approximately 230 kHz. In high repetitive mode, the overheating of the transistors and the resistors on PCB can be quite significant, and it is important to take appropriate heat dissipation measures for the reliability of the components. As shown in Fig. 2(c), we use four 1.8 kΩ/2 W resistors in each charging circuit to reduce the heat power density of the isolation resistor. The print circuit board has also been hollowed at the location of resistors to enlarge the heat dissipation surface. As for the avalanche transistor, the rated power is 330 mW. It means that the heat density can reach as high as 300 W/cm^2 in the *b-e* die region. A special design is needed for the avalanche transistor operating at a high repetition rate. The detailed analysis of the power dissipation of avalanche transistors at a high repetition rate will be discussed in Section III.

B. Experimental Platform

Fig. 4 shows the experimental platform of the avalanche transistor pulse generator and the schematic diagram of different cooling techniques. During the experiment, a dc power source with enough power capacity was used to apply voltage to the 60-stage pulse generator. We also developed another pulse generator with a fast front, high amplitude, and small half-width to trigger the first stage avalanche transistor, which benefits the generation of high-repetition-rate pulse and reducing the time base jitter [25]. A trigger signal generator (DG 645) was applied to control the operation frequency. The output high voltage pulse was attenuated by an attenuator, and the oscilloscope recorded the waveform. The load impedance was 50 Ω. An infrared thermal imager was applied to acquire the temperature distribution of the components. To determine the temperature transient process of components, we pasted K-type thermocouples with a diameter of 100 μm onto the selected transistor and charging resistor surface with heat conductive. The pasted thermocouples were deposited to form a small droplet (<0.5 mm × 0.5 mm) to minimize the influence of transistors heat dissipation and reduce the error on the temperature measurement. However, the temperature error could still be large for the high heat flues condition, but the temperature change tendency under different cooling techniques can be qualitatively compared. During the experiment, the avalanche transistors in the 5th stage, 20th stage, 40th stage, and 55th stage were selected as the sample points. The multichannel temperature monitor recorded the temperature at different locations simultaneously. The thermocouples and the record channel were calibrated before the experiments.

C. Cooling Technique

Three cooling techniques have been applied to the high repetition rate pulse generator, including FAC, SPIC, and two-phase immersion cooling. The schematic diagram of different cooling techniques is shown in Fig. 4(b)–(d), and the description of each system are as follows.

1) FAC *system description*: In FAC, the PCB is mounted on a heat sink. Before the experiment, different types of fans' positions have been tested, and the optimized plan of FAC is adopted. Two fans (65 W) are placed above the circuit

TABLE I
PROPERTIES OF DIFFERENT DIELECTRIC FLUIDS

Property	Novec 7000	Novec 7100	Novec7200	Novec 7300	Novec 7500	FC-72	Transformer oil
T_b [°C]	34	61	76	98	128	56	~130
$T_{critical}$ [°C]	165	195	210	243	261	176	/
P_v [kPa]	65	27	16	5.9	2.1	30	/
ρ [kg/m^3]	1400	1510	1420	1660	1614	1680	874
k [W/(m·k)]	0.075	0.069	0.068	0.063	0.065	0.057	0.128
h @ T_b [kJ/kg]	142	112	119	102	89	88	/
c [J/(kg·k)]	1300	1183	1220	1140	1128	1100	1898
σ [mN/m]	12.4	13.6	13.6	15.0	16.2	10.0	48
v [cSt]	0.32	0.38	0.41	0.71	0.77	/	10.12
U_b@**0.1in gap** [kV]	40	28	28	40	40	40	35
ε	7.4	7.4	7.3	6.1	5.8	1.8	2.2-4.5
ρ [Ohm/cm]	10^8	10^8	10^8	10^{11}	10^8	10^8	/
GWP	420	297	59	210	100	9000	/

board, and the transferred airflow is perpendicular to the component. Although further increasing the number and power of fans could improve the FAC cooling effect, the bulky system and energy cost cannot be accepted.

2) SPIC *system description:* In SPIC, the circuit board is arranged in an aluminum vessel and submerged in the transformer oil. Before the experiment, different oil has been tested, and the Kunlun KI50X is finally adopted for the low kinematic viscosity and better cooling effect. A fan is placed at the side of the vessel in the longitudinal direction.
3) *Two-phase immersion cooling system description:* In the TPIC system, the circuit board is arranged in the aluminum vessel and submerged in the dielectric coolant. An aluminum plate is placed tightly on the top of the vessel to minimize the leakage of the coolant. The sealed vessel is cooled by the same fan used in the TPIC. When the coolant absorbs heat from the heating elements, the liquid starts to vaporize. This hot vapor is converted to liquid in the condensing area (the top plate and the vessel wall), where heat is finally transferred to the ambient air. The liquid coolant must possess the dielectric strength needed to provide electrical isolation, especially for the high voltage pulse generator application. Moreover, other properties, including boiling point and latent heat, also need to be considered. Among the different dielectric liquids, the perfluorocarbons and hydrofluoroethers (HFEs) developed by the 3M Corporation provide a mix of properties, such as low wetting angles on most engineering surfaces, relatively low critical pressures, and specific heats [7], [26]. Five different coolants, including Novec 7100, Novec 7200, Novec 7300, Novec 7500, and FC-72, were selected and tested during the experiments. The property parameters of different coolants are listed in Table I [27]–[29].

The output characteristic including amplitude, amplitude jitter, time base jitter, and the temperature distribution under FAC, SPIC, and TPIC are studied, respectively. Then the TPIC with different coolants is experimentally compared. In order to avoid the irreversible thermal destruction of avalanche transistors due to overheating, the operation time is no more than 180 s. When the temperature of the transistor exceeds 95 °C, the operation should be interrupted. In TPIC, the amount of the coolant was ensured to be the same before each experiment.

III. ANALYSIS OF POWER DISSIPATION AND THERMAL DESTRUCTION PROCESS UNDER REPETITIVE MODE

Before the experimental characterization of the different cooling techniques is presented, the theoretical analysis of the Joule heating process and the estimation of power dissipation of the components will be discussed in this section. It will underline the importance of the implementing of cooling technique in the high voltage and high repetition rate avalanche transistor pulse generator.

The heat of the pulse generator is mainly generated from the resistor and avalanche transistor by Joule heating during the charging and discharging process. Fig. 5 shows the schematic of the charging process, discharging process, and the power dissipation process in parallel charging Marx circuit.

1) *Power dissipation of charging resistor*

As shown in Fig. 5(a), the main capacitors are charged by the currents flowing along the blue lines in the charging process. The peak charging current I_{m} can be calculated according as

$$I_m = n \cdot U_{\mathrm{c}}/R_{\mathrm{c}} \tag{1}$$

in which U_{c} represents the supply voltage, R_{c} is the total charging resistance, n is the circuit stage. Thus, the charging current conducted in every charging resistor is approximately

$$i_0(t) = I_{0\mathrm{m}} \exp\left(-\frac{t}{\tau_1}\right) \tag{2}$$

where $I_{0\mathrm{m}}$ is the peak charging current, and it is calculated as $I_{0\mathrm{m}} = I_{\mathrm{m}}/n = U_{\mathrm{c}}/R_{\mathrm{c}} = 4.44\times10^{-2}$ A, and the time constant $\tau_1 = R_c \cdot C = 7.2 \times 10^{-7}$s. Then, the average power dissipation P_{R1} on a charging resistor with frequency f during the charging process can be calculated as

$$P_{\mathrm{R1}} = f \cdot \int_0^{t_0} {i_0}^2 \times \frac{R_{\mathrm{c}}}{4} dt \tag{3}$$

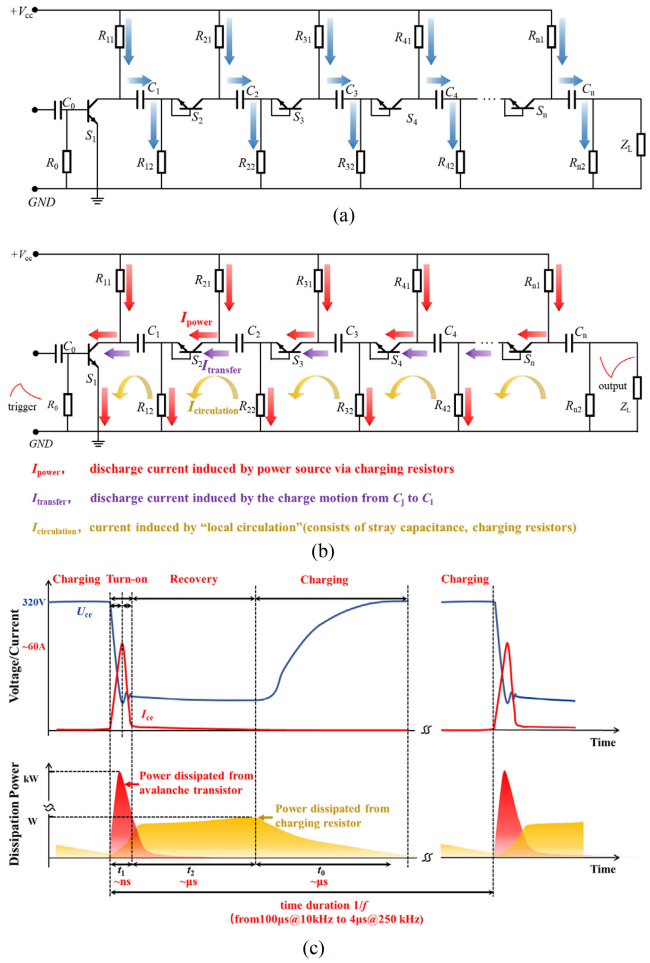

Fig. 5. Schematic of the charging, discharging, and power dissipation process. (a) Current flow path in the charging process. (b) Current flow path in discharging process. (c) Power dissipation in different processes within a period.

which determines that $P_{\mathrm{R1}} = f \times 1.28 \times 10^{-6}$ W. During the pulse forming process, with the switch closed, the current flowing through the charging resistor is induced by power source I_{power} and the local circulation current I_{cir}, as shown in Fig. 5(b). Considering the time of the pulse formation process is relatively short, the equivalent power in this stage can be neglected.

It should be mentioned that the avalanche transistor cannot shut down immediately after the pulse formation process due to the residual charge in the PN junction. During this period (recovery time), the transistor can maintain the conduction state, with a conductive voltage drop U_{on} and a resistance R_{on}. In this recovery stage, the current will form through the charging resistor, and it can be calculated as

$$i_1(t) = \frac{U_{\mathrm{c}} - U_{\mathrm{on}}(t)}{R_{\mathrm{c}} + R_{\mathrm{on}}(t)} \approx \frac{U_{\mathrm{c}}}{R_{\mathrm{c}}}. \tag{4}$$

Then the power dissipated on charging resistor P_{R2} with a repetitive frequency f during voltage recovery stage can be calculated according to

$$P_{\mathrm{R2}} = f \cdot \int_0^{t_2} i_1 \times^2 \times \frac{R_{\mathrm{c}}}{4} dt \tag{5}$$

in which the voltage recovery stage lasts about 2.0 μs (measured at 1 Hz, 25 °C) according to the measurement waveform of U_{c}. And it determines that $P_{\mathrm{R2}} = f \times 7.11 \times 10^{-6}$ W. Finally, we can get the average dissipated power P_{R} of a charging resistor according to (6).

$$P_{\mathrm{R}} = P_{\mathrm{R1}} + P_{\mathrm{R2}} = f \times 8.39 \times 10^{-6} \quad \mathrm{W}. \tag{6}$$

2) *Power dissipation of avalanche transistor*

During the switch turn-ON process, the voltage across the emitter and collector (U_{ce}) collapses while the avalanche current (I_{ce}) dramatically increases. Theoretically, the transistor's power dissipation can be calculated by $U_{\mathrm{ce}} \times I_{\mathrm{ce}}$. However, the I_{ce} and U_{ce} are difficult to measure directly on the PCB circuit due to the ultrafast process. Moreover, the time phase difference always causes a huge error in the power calculation. During discharging process, the current flowing through each transistor approximately equals that through the load. Thus, the power dissipation of transistors in discharging process, P_{R1}, can be expressed as

$$P_{\mathrm{Q1}} = f \cdot \int_0^{t_1} \left(\frac{u(t)}{R_{\mathrm{L}}} \right)^2 \cdot r dt \tag{7}$$

where u(t) is the output voltage and the R_{L} is the equivalent load resistance 50 Ω, and the r is the equivalent ON-state resistance of avalanche transistor [30]. According to the FMMT417 datasheet, the maximum continuous current is 500 mA, and the power dissipation is 330 mW, and the conductive resistance can be estimated to be 1.32 Ω. Furthermore, u(t) can be obtained from the recorded waveform on the oscilloscope. Applying the waveform shown in Fig. 3, we can get that $P_{\mathrm{Q1}} = f \times 1.13 \times 10^{-6}$ W. In the voltage recovery stage, the dissipated power P_{Q2} can be calculated as

$$P_{\mathrm{Q2}} = f \cdot \int_0^{t_2} {i_1}^2 \cdot R_{\mathrm{on}}(t) = f \cdot \int_0^{t_2} P_{\mathrm{r}} dt. \tag{8}$$

However, most of the work only focused on the power dissipation on the turning-ON process [30]. Indeed, the P_{R2} can play an important role in the temperature rising. According to *Duan et al.*, the residual carriers of avalanche transistors initiate a weak but important avalanche multiplication. Even at a current of ~several mA and a voltage of ~100–300 V, this multiplication will correspond to 1 W heating power. Thus, within a time interval of several microseconds, more thermal energy will be generated during the voltage recovery stage than that earlier accumulated during high-current nanosecond-range switching [19], [24], [31]. According to the measurement of U_{c}, the recovery time lasts for about 2.0 μs (measured at 1 Hz, 25 °C). Thus, we can obtain that the average power dissipation during the voltage recovery stage is $P_{\mathrm{Q2}} = f \times 2 \times 10^{-6}$ W. And

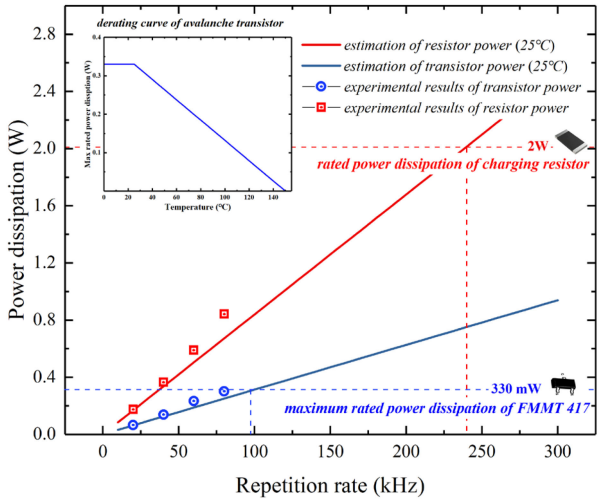

Fig. 6. Estimated power dissipation of avalanche transistor and charging resistors under different repetition rate (under 25 °C) and the experimental results of transistor and resistor power at 20, 40, 60, and 80 kHz.

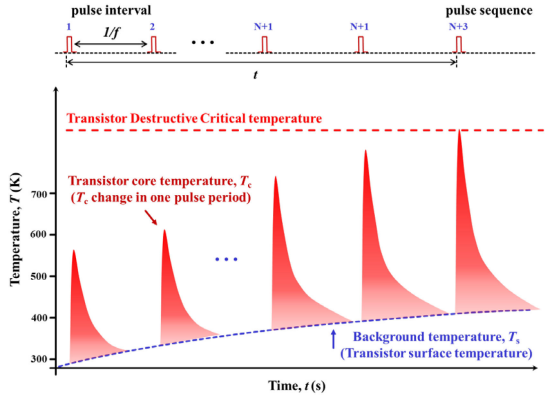

Fig. 7. Schematic of temperature rising and thermal destruction process under repetitive operation mode [24].

the total transistor power dissipation under a repetition rate f is

$$P_{\mathrm{Q}} = P_{\mathrm{Q1}} + P_{\mathrm{Q2}} = f \cdot 3.13 \times 10^{-6}\mathrm{W}. \tag{9}$$

With (6) and (9), the equivalent power of transistor and resistor at a different frequency can be calculated, and they are shown in Fig. 6 with solid lines. It can be seen that the power dissipation increases with the operating frequency. Since the resistance is kept constant in the calculation, the power dissipation is almost linear with the operating frequency. Under this condition, the estimated maximum repetition rate of the avalanche transistor is around 100 kHz. However, it is worth emphasizing that the resistance of the charging resistor, ON-state resistance, and the avalanche transistor's recovery time are all temperature-dependent parameters. With the temperature of components rising, the resistance and recovery time will increase. Therefore, the calculation results with (1)–(9) will underestimate the dissipation power of components under higher temperatures. To evaluate the power dissipation under the repetitive mode, the pulse generator was operated at 20, 40, 60, 80 kHz, respectively, without a cooling technique applied. The output waveform, recovery time were measured. In order to estimate the equivalent resistance of the transistor, a simplified circuit model has been utilized, as

$$n \times V_{cc} \times \frac{R_{\mathrm{load}}}{n \times r + R_{\mathrm{circuit}} + R_{\mathrm{load}}} = U_{\mathrm{output}}. \tag{10}$$

In this equation, the n is the stage of the pulse generator ($n = 60$), R_{load} is 50 Ω, R_{circuit} is the equivalent circuit impedance beyond the resistance of avalanche transistor during the pulse formation (the impedance of inductance, and the other parameters which cause the amplitude loss) and the U_{output} is the amplitude of the output pulse. According to the voltage amplitude and the ON-state resistance of the avalanche transistor at 25 °C, R_{circuit} can be estimated. Generally, the R_{circuit} almost remains constant. Thus, the ON-state resistance can be determined by replacing the U_{output} with corresponding voltage amplitude at a different repetition rate. The experimental values of the power dissipation under the different repetition rates are shown in Fig. 6 with blue circle and red square symbols.

It can be seen that, due to the increase of the recovery time and ON-resistance (20 kHz, 2.1 μs, 1.45 Ω; 40 kHz, 2.2 μs, 1.65 Ω; 60 kHz, 2.4 μs, 1.98 Ω; 80 kHz, 2.6 μs, 2.32 Ω.), the dissipation power of transistor and resistor is higher than the estimation results at 25 °C. With the further increase of the repetition rate, the power dissipation of the avalanche transistor will exceed the rated power and finally result in overheating. In the experiment, the maximum frequency of the pulse generator is 80 kHz, and transistor destruction will appear with a higher frequency or a longer operation time. The calculation indicates that the maximum power dissipation of the transistor is 301.38 mW, which is close to the rated power. Although the measurement technique and model simplification limit the accuracy of the calculation result, it can fit the experimental observation well. The analysis above can be used for the estimation of heat power dissipation under different frequencies.

The junction temperature of the avalanche transistor under repetitive operation mode can be related to the power dissipation P_{L} by the expression [32]

$$T_{\mathrm{j}}(t) = T_0 + \int_0^t P_{\mathrm{L}}(\tau) \cdot \frac{dR_{\theta\mathrm{ja}}(t-\tau)}{dt} d\tau \tag{11}$$

where T_0 indicates the ambient temperature, $P_{\mathrm{L}}(\tau)$ is the dissipated power, and the $R_{\theta\mathrm{ja}}$ is the junction to the ambient thermal impedance of the transistor. The temperature in the "hot zone" of the transistor structure could reach a peak value of a few hundred Kelvin. [19] While it would not lead to destruction due to the short duration. After the switching process, the temperature of the hot zone will gradually cool down to room temperature. If further increasing the operation frequency, the diffusion time constant becomes comparable to the pulse interval, the temperature in the "hot" domain will grow from pulse to pulse, which may lead to the destruction of the device. The damage process of the avalanche transistor circuit due to overheating under repetitive frequency conditions can be depicted in Fig. 7. It is obvious that thermal accumulation grows fast with the pulse

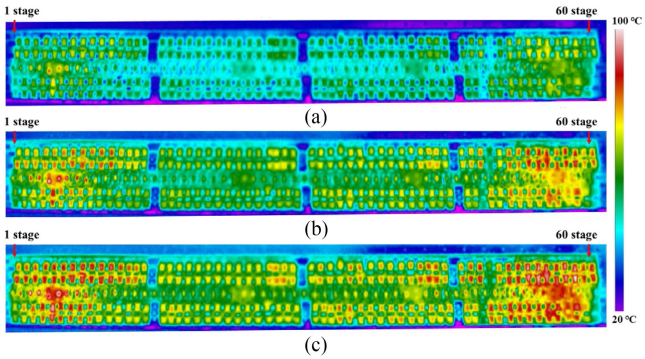

Fig. 8. Infrared thermograph of the pulse generator under different frequency.

cycles. An effective cooling method is indispensable for the high repetition rate pulse generator.

IV. Experimental Results and Analysis

A. Comparison of Temperature Rising Characteristics With Different Cooling Method

The avalanche transistor circuit with the different cooling techniques was compared with the experiment platform, and the temperature distribution was studied with infrared imaging. In order to avoid overheating damage caused by the long-term operation, the thermographs were taken after a burst mode operation for 60 s during the experiments. Fig. 8 shows the thermographs of the pulse generator without the cooling technique applied. It can be noted that more heat will be generated under the repetitive rate of 80 kHz ($\sim 4.8 \times 10^6$ pulse generated in the 60 s). The hot spot temperature has exceeded 95 °C, which is close to the critical temperature. Further increasing the frequency will cause thermal damage to the avalanche transistors. The maximum temperature difference is nearly 50 °C (98 °C in the 55th stage and 50 °C in the 23rd stage). Avalanche transistors in the first several stages operate in the conduction mode of "overvoltage switching-ON", and they suffer from the thermal destruction caused by current filamentation due to the lower overvoltage coefficient. While the working state of avalanche transistors near the end of the circuit is quite different; and the current rising rate can be much higher. Moreover, the mismatch of the circuit resistance and the load resistance will induce the voltage wave reflection, which also aggregates the heat dissipation.

Due to the inhomogeneous distribution of the temperature, it was found that the avalanche transistors in the first stage and last stages are more prone to thermal damage during the experiment. The thermograph shows that the avalanche transistor in the 55th stage has the highest temperature. Thus, the 55th stage transistor temperature was recorded to estimate the overall reliability of the pulse circuit. The transistor temperature rising process with FAC, SPIC, and TPIC (with FC-72) under different frequencies has been acquired, as shown in Fig. 9(a)–(c), respectively. The pulse generator continues operating until the steady temperature of the transistor is reached (the fluctuation of temperature is less than 0.2 °C within the last 5 s) or the overheating occurs (>95 °C). Generally, the TPIC can achieve much lower

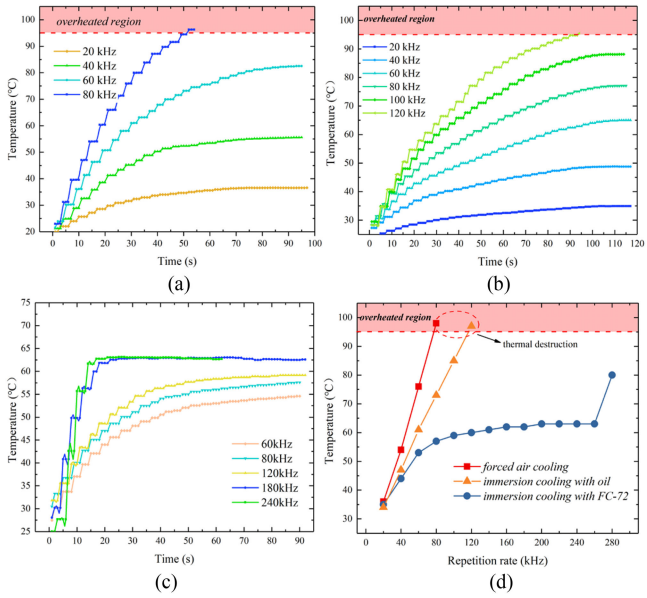

Fig. 9. Comparison of the temperature rising characteristics of 55th stage transistor with different repetition rates and different cooling methods. (a) With FAC, (b) with SPIC, (c) with TPIC, and (d) direct comparison of steady temperature with FAC, SPIC, and TPIC.

avalanche transistors temperature than FAC and SPIC. At 80 kHz, the temperature of transistors under FAC has exceeded 98 °C at the 50 s and continues increasing, while the steady temperature of transistors under SPIC is around 76 °C. The TPIC can reduce the steady temperature to around 57 °C. TPIC also shows the capability to reduce the time response of the temperature rising process. The temperature rising characteristics as a function of time show that it usually takes a longer time to reach the stable temperature with increasing repetition rate when FAC and SPIC are adopted. The transient process of temperature rising, however, obviously shortens with TPIC at a high repetition rate. As shown in Fig. 9(c), the transition time is reduced from 60 to 15 s with the frequency increasing from 60 to 240 kHz, which implies that the higher power dissipation leads to phase change of the coolant and enhances the cooling effect.

The steady-state temperature of the 55th stage transistor with FAC, SPIC, TPIC under different frequencies is shown in Fig. 9(d). The experimental results show that the TPIC method can significantly improve the repetitive frequency operation capability of the pulse generator. Avalanche transistors with the TPIC technique can achieve a large operation range of repetition rate from 100 to 260 kHz while the temperature effectively controlled at around 60 °C. When the power of the avalanche transistor is further increased to 280 kHz, the TPIC method cannot provide sufficient heat dissipation capacity, and the temperature of the avalanche transistors abruptly increased, the coolant boiled intensely. Thermal destruction finally occurred in long-term operation. More details of the TPIC process will be discussed in Section V.

Comparing the temperature of transistors in the 5th stage, 20th stage, 40th stage, and 55th stage with the different cooling

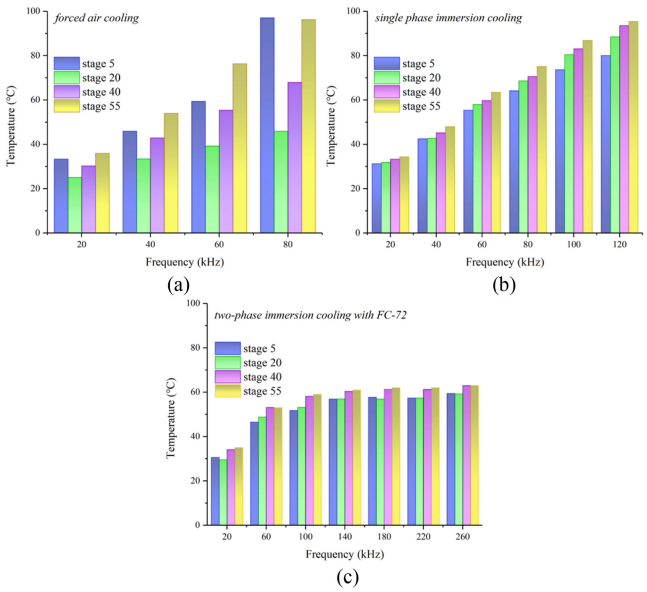

Fig. 10. Comparison of the temperature distribution with different cooling methods at different repetition rates. (a) FAC. (b) SPIC. (c) TPIC.

techniques are shown in Fig. 10. In SPIC system, heat transfer is improved due to the natural liquid convection. The temperature difference is reduced compared with FAC. When operating at a low repetition rate, the maximum temperature difference of the avalanche transistors can be effectively limited to 5 °C. When the operating frequency is further increased, since natural convection heat transfer is difficult to meet the heat dissipation requirements of high heat flow, the maximum temperature difference increases to 10 °C.

TPIC technique can also benefit pulse generators in maintaining even temperature distribution. With TPIC, the boiling effect provides the possibility of increasing heat absorption per unit volume of fluid and higher heat acquisition effectiveness (i.e., the amount of heat absorbed by a unit of flow relative to its maximum theoretical capacity). This latent heat benefit is coupled with the improved convection due to buoyancy-driven bubble formation, multiphase tabulation, and mixing within the heat transfer region. The resultant heat transfer coefficients from a two-phase flow can be an order of magnitude greater than equivalent single-phase forced convection [28]. The results indicate that TPIC can effectively improve the uneven temperature distribution whether the pulse generator operating at low frequency or high frequency, and it undoubtedly improves the reliability of the avalanche transistors.

B. Comparison of Output Characteristic With FAC, SPIC, and TPIC Techniques

Amplitude stability and time base stability are important parameters of the pulse generator, determining the Radar measurement accuracy, pulse synthesis efficiency [25], trigger effect [6]. The amplitude jitter U_{r} is defined as

$$U_r = \frac{U_{\max} - U_{\min}}{U_{\max} + U_{\min}} \times 100\% \tag{12}$$

TABLE II
COMPARISON OF OUTPUT PARAMETERS WITH DIFFERENT COOLING TECHNIQUE

(a) 20 kHz

Cooling method	pulse drift (ps)	Voltage amplitude jitter (%)	temperature (°C)
FAC	29	1.6	36
SPIC	30	1.4	35
TPIC	30	1.4	35

(b) 40 kHz

Cooling method	pulse drift (ps)	Voltage amplitude jitter (%)	temperature (°C)
FAC	66	3.3	55
SPIC	61	1.8	49
TPIC	55	1.6	44

(c) 60 kHz

Cooling method	pulse drift (ps)	Voltage amplitude jitter (%)	temperature (°C)
FAC	142	5.2	83
SPIC	110	3.2	65
TPIC	78	1.7	53

(d) 80 kHz

Cooling method	pulse drift (ps)	Voltage amplitude jitter (%)	temperature (°C)
FAC	340	6.5	98 (overheated)
SPIC	205	4.3	77
TPIC	95	1.8	57

(e) 100 kHz

Cooling method	pulse drift (ps)	Voltage amplitude jitter (%)	temperature (°C)
FAC	/	/	/
SPIC	320	6.0	88
TPIC	118	1.8	59

where $U_{\max}$ and $U_{\min}$ are the maximum and minimum values of pulse amplitude in the period of 90 s. The time base pulse drift is defined as the *Range* of the time delay t_{delay} (the time interval between the trigger pulse and output pulse), and it was recorded in a period of 30 s during the experiment

$$t_{\mathrm{r}} = \max(t_{\mathrm{delay}}) - \min(t_{\mathrm{delay}}). \tag{13}$$

The results of amplitude jitter and pulse drift of pulse generator with the different cooling methods are shown in Table II. According to Yuan *et al.* [33], avalanche transistors are sensitive to temperature (with the increase of temperature, the reverse saturation current of the collector I_{CBO} approximately doubles for every 10 °C, and the emitter junction voltage decreases by 2 mV for every 1 °C). As the temperature rises, the static operating point of the avalanche transistors will change. The delay time increases, and the peak voltage of the output pulse is reduced. As shown in Table II, there is little difference between the different cooling methods at 20 kHz. However, with the repetition rate increasing to 80 kHz, the pulse drift increases significantly, and it exceeds 200 ps in FAC and SPIC. TPIC shows an obvious advantage in controlling the output stability at a high repetition rate. When the repetition rate increases to 100 kHz, the pulse drift is only 118 ps, and the amplitude jitter is relatively small. The high stability of the pulse generator could be achieved with the effective cooling effect of TPIC, and it is important in applications that low-time jitter and amplitude jitter are required.

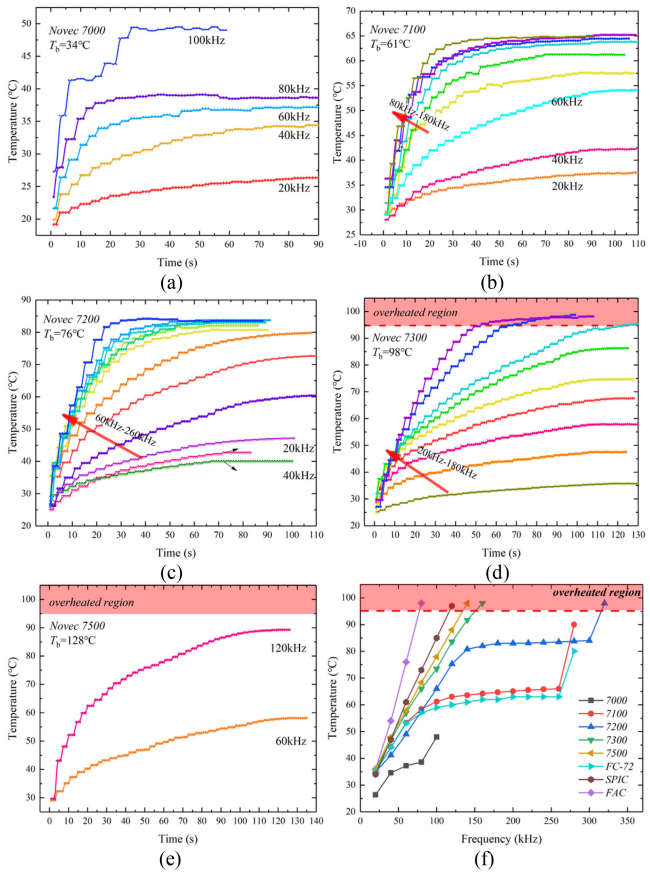

Fig. 11. Temperature rising characteristics of 55th stage avalanche transistor. (a) Novec 7000. (b) Novec 7100. (c) Novec 7200. (d) Novec 7300. (e) Novec 7500. (f) Comparison of repetition rate with different coolants.

TABLE III
COMPARISON OF OUTPUT PARAMETERS WITH DIFFERENT COOLANTS

(a) 60 kHz

Coolant	Time-base jitter (ps)	Voltage amplitude jitter (%)	Steady temperature (°C)
7000	67	1.1	37
7100	76	1.4	54
7200	87	1.7	49
7300	90	2.3	57
7500	96	2.0	58
FC-72	78	1.7	53

(b) 120 kHz

Coolant	Time-base jitter (ps)	Voltage amplitude jitter (%)	Steady temperature (°C)
7000	/	/	>95(overheated)
7100	110	2.4	64
7200	117	3.0	75
7300	140	3.4	86
7500	256	4.2	89
FC-72	118	1.9	60

(c) 180 kHz

Coolant	Time-base jitter (ps)	Voltage amplitude jitter (%)	Steady temperature (°C)
7000	/	/	/
7100	254	2.8	64
7200	583	3.1	83
7300	/	/	>95(overheated)
7500	/	/	>95(overheated)
FC-72	267	1.9	62

C. Temperature Rising and Output Characteristics of TPIC With Different Coolant

In order to reach a coolant selection standard, different dielectric fluids were applied as immersion fluids and tested experimentally, including Novec 7000, Novec 7100, Novec 7200, Novec 7300, Novec 7500, and FC-72. The properties of the dielectric fluids are shown in Table I. The temperature rising process and the comparison of the steady temperature under different repetition rates are shown in Fig. 11. Fig. 11(a)–(e) shows a similar tendency in the time response of the temperature rising process. Whatever coolant is selected, the temperature of the avalanche transistor rising with the increasing of repetition rate until the boiling point of the coolant is reached. The increasing power dissipation reduces the time required to reach a stable temperature. As the boiling point of the coolant increases, the temperature response time becomes longer. When the Novec 7000 was utilized, it only took 15 s to reach the steady-state temperature of 38.6 °C, while at the same operating frequency of 80 kHz, the temperature of the pulse generator with Novec 7500 kept increasing in 100 s. According to the property data shown in Table I, we can find that the different type of coolant has the almost similar latent heat and specific heat capacity. It indicates that the temperature rise is determined by the total amount of heat energy absorbed during the phase change process. The dielectric liquid with a lower boiling point is more suitable for applications that require the rapid establishment of stable operating parameters. The comparison of steady-state temperature with different coolants and different frequencies is shown in Fig. 10(f). During the experiment, the transistor frequency was increased until the temperature entered the overheated region (T_s >95 °C). The curves depict the regime of single-phase natural convection as well as the pool boiling regime. For the dielectric fluids, critical heat flux (CHF) is reached when the heat density is higher than the heat dissipation capacity of the phase change, which will lead to the fast dry out of the coolant and the dramatic rise of the device temperature. In the experiment, the CHF occurred in FC-72 (at 280 kHz), Novec 7100 (at 280 kHz), and Novec 7200 (at 320 kHz).

The time-base jitter and voltage amplitude of the output waveform with different coolants under 60, 120, and 180 kHz are listed in Table III. According to the analysis in Section IV-B, the reverse saturation current and the emitter junction voltage of avalanche transistors are sensitive to the temperature. The lower operation temperature benefits reducing the time base jitter and voltage amplitude jitter. When operating at 60 kHz, there is little difference in time base jitter and voltage amplitude jitter with four dielectric fluids. The time-base jitter can be effectively controlled below 100 ps, and the voltage amplitude jitter is lower than 2.5%. While the frequency is 180 kHz, the time base jitter of the Novec 7200 increases to 583 ps, which is unacceptable in pulse synthesis application.

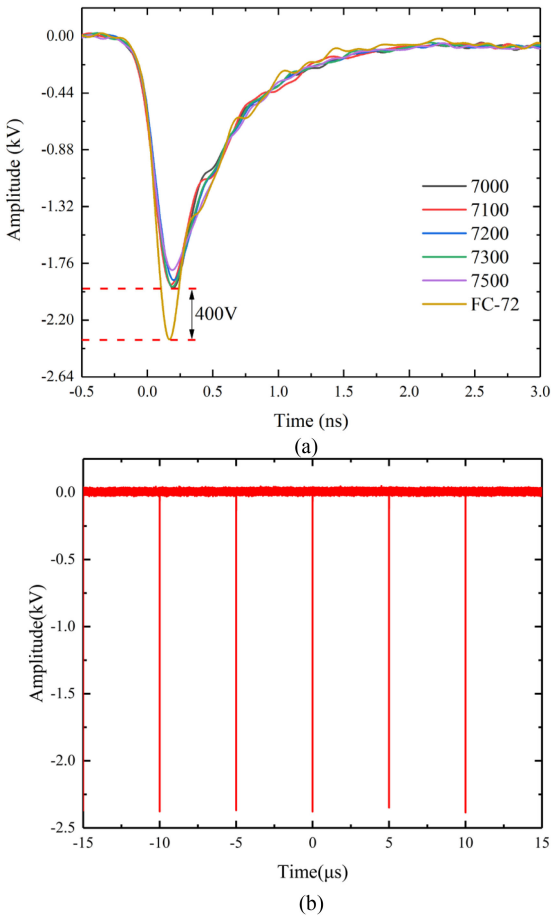

Fig. 12. Output waveform of the pulse generator with TPIC technique. (a) Comparison of voltage waveform with different coolant. (b) Repetitive pulses at 200 kHz with FC-72 coolant.

D. Output Parameters Validation of Pulse Generator With TPIC Technique

Fig. 12(a) shows the output voltage waveform with different coolants. It is apparent that the output amplitude is lower than that in the air, as shown in Fig. 3. When the pulse rise time is reduced to the order of subnanosecond, the effect of distributed parameters and traveling wave process cannot be ignored in the circuit. The pulse formation process is a propagation process of quasi-TEM waves in the microstrip line. It is desirable that the liquid's dielectric constant can be close to unity to avoid significant propagation delays. However, the dielectric constant is always greater than 1. The introduction of fluorinated liquid will increase the equivalent dielectric constant, and it also reduces the characteristic propagation velocity, $V_p = c/\sqrt{\varepsilon_e}$, where c is the light velocity, and ε_e is the dielectric constant. Besides, the wave impedance will decrease due to the increase of the distributed capacitance of the microstrip line, resulting in the mismatch with the terminal impedance. Thus, the longer propagation time and mismatch of the impedance will reduce the output voltage efficiency [10], [14]. In addition, since the dielectric loss of the microstrip line is positively related to the tangent of the loss angle, the high-frequency components are attenuated greatly. The rise time of the output waveform with the TPIC technique increases.

Based on the performance test results, it can be concluded that the pulse generator with coolant Novec 7200 shows the best performance from the view of the allowable operating range of repetition rate, and the maximum repetition rate could reach 300 kHz. While on the time base jitter and voltage amplitude jitter parameters, Novec 7100 and FC-72 are superior to the other coolant. The steady temperature can be effectively controlled below 65 °C, and a lower time-base jitter can be obtained, which is suitable for the application required for high reliability and stability. Due to the lower dielectric constant, the output voltage amplitude with FC-72 ($\varepsilon = 1.8$) is larger than other coolants. Considering the output amplitude and maximum repetition rate, FC-72 shows a balanced performance. It should be mentioned that the main drawback of coolant FC-72 is the relatively high GWP value. The sealing of the vessel and careful treatment on coolant transferring are required, which can much reduce the leakage due to vaporization.

Finally, the FC-72 is selected as the coolant. The long-term operating performance of the avalanche transistor pulse generator with TPIC is tested. The output peak voltage reaches 2350 V, with the rise time of 180 ps and the FWHM of 530 ps. Fig. 12(b) shows the waveform at a frequency of 200 kHz. It can be seen that the waveform is stable, and the repeatability is excellent. With TPIC applied, the pulse generator can work stably at 200 kHz for more than 30 min, and the burst repetition rate could be 260 kHz within 1 min. The maximum operating frequency is 3.25 times higher than that with the FAC technique.

Table IV shows the comparison of output parameters in previous literature, which mainly focuses on the pulse generator's high repetition and voltage amplitude performance. In order to evaluate the output performance of the pulse generator combined with repetition rate and amplitude, a factor k is defined

$$k = f \cdot {U_{\rm p}}^2/R \tag{14}$$

where $U_{\rm p}$ is the peak voltage of the output pulse, f is the pulse repetition, and R is the load impedance. The k factor of the pulse generator can be greatly extended by adopting the TPIC technique. These experimental results show that the heat dissipation capacity has greatly improved by applying the TPIC technique to the avalanche transistor pulse generator. High output amplitude and high repetition rate are obtained, and reliable long-term operation can be acquired due to the effective temperature controlling of the components.

V. Discussion

A. Two-Phase Immersion Cooling Process and the Desirable Operating Region

When applying a two-phase immersion cooling technique to the high-power repetitive pulse generator, one of the key factors is the highest temperature. The "hot spot" that is registered at a certain point in the package should not exceed the specified rating value. If the temperature rises above the allowable value, the reliability of components is threatened. According to the experiment, the temperature rising characteristics of the

TABLE IV
COMPARISON OF OUTPUT PARAMETERS OF AVALANCHE TRANSISTORIZED SUBNANOSECOND PULSE GENERATORS

First author	Year	Pulse width/ns	Rise time/ps	PRF/kHz	Amplitude/kV	*k*/kHz·MW
B. Liang[8]	2005	2	400	1	2.6	0.14
P. Krishnaswamy[34]	2007	1.3	800	200	1.1	4.84
X. Yuan[35]	2010	1.6	250	30	2	2.40
Y. Zhang[36]	2017	1.3	400	100	0.366	0.27
M. Gao[14]	2019	0.3	160	300	1.1	7.26
C. Li[10]	2019	0.35	150	10	3.1	1.8
This work	2021	0.54	180	200	2.35	22.1

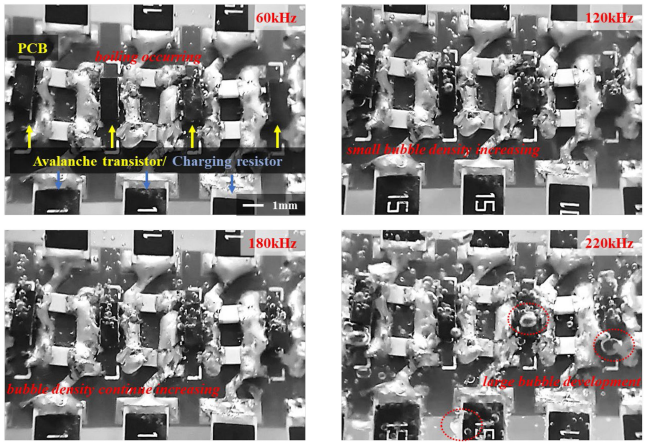

Fig. 13. Photograph of the bubble state of several boiling stages under different repetition rates.

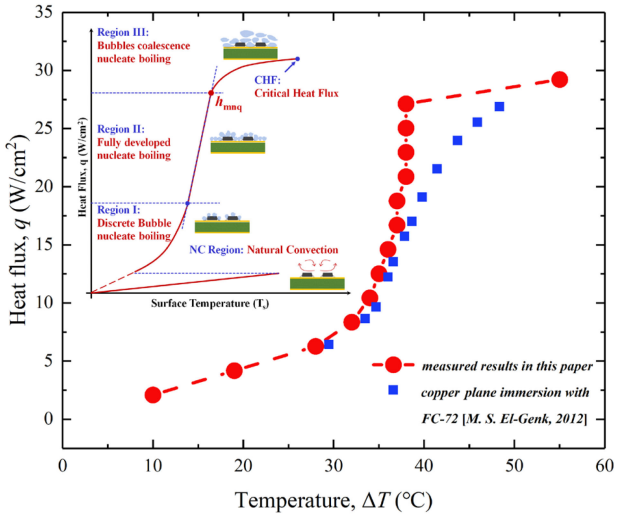

Fig. 14. Power dissipated per transistor as a function of the temperature difference between the top surface of the transistor and the ambient fluid temperature.

transistor is dependent on the boiling point and the dissipation power. Thus, it is necessary to determine the correspondence between the coolant state, phase change process, and heat flux density.

The phase change process of the dielectric liquid is closely related to the bubble formation and transition process. Fig. 13 shows the photographs of nucleate boiling of FC-72 on the pulse generator under different repetition rates from 60 to 220 kHz. At 60 kHz, the bubbles nucleation occurs at a few isolated sites on the avalanche transistor surface. Increasing the surface heat flux increases the number of active sites for bubbles nucleation and the population of the growing bubbles on the surface. It also increases the coalescence of the departing and growing bubbles at and near the surface. Following boiling incipience, the nucleate boiling heat transfer rate increases with increased heat flux.

With the operating frequency increased to 220 kHz, it shows that the number of vapor bubbles growing and departing from the surface increases. Large bubbles also develop and release from the surface of charging resistors. While the induced mixing in the boundary layer by the rising and detaching vapor bubbles increases the nucleate boiling heat transfer rate, the added resistance due to vapor accumulation in the boundary layer increases the surface temperature. This decreases the nucleate boiling heat transfer coefficient and increases the boiling thermal resistance. After film boiling is established, very high heat transfer coefficients can be reached [29]. The analysis above indicates that the desired operating region for the avalanche transistor circuit lies in the region where the heat flux can be effectively removed with the bubbles with a moderate temperature increase.

According to the traditional theory, the phase change process mainly consists of five stages: natural convection, the discrete bubble nucleate boiling, the fully developed nucleate boiling, the bubble coalescence nucleates boiling region, and finally ending with CHF [29]. The desirable operating points are far enough from the CHF (near the end of Region II), where the maximum nucleate boiling heat transfer h_{mnq} occurs. Based on the measurement results of the surface temperature, the heat flux as a function of the surface superheat (temperature difference between avalanche transistor surface and coolant) is calculated and shown in Fig. 14. In addition, the typical pool boiling curve of dielectric liquids is illustrated in Fig. 14 as a subplot [29], [34]. It indicates that the discrete bubble nucleate boiling mainly develops when the heat flux is lower than 10 W/cm^2, corresponding to a repetition frequency of 100 kHz. As the heat flux increases, it steps into Region II, and the temperature difference only changes within a small range. The maximum nucleate boiling heat transfer coefficient h_{MNB} shows

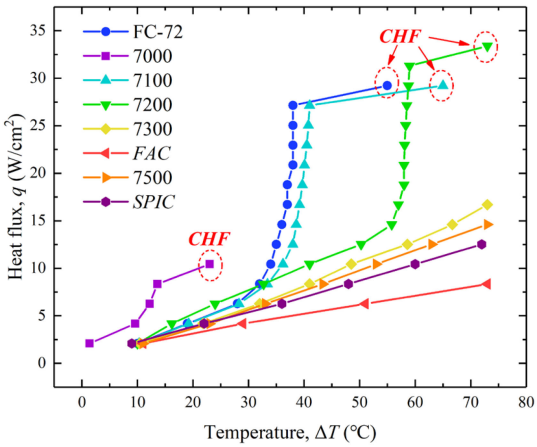

Fig. 15. Heat flux curve with the increase of superheat of avalanche transistors with different coolant.

up when the surface superheats nearly increases to 40 °C, and the corresponding heat flux is 27.1 W/cm^2. If the repetition rate is increased further, the surface superheats rapidly, and the CHF occurs. The measurement results of nucleate boiling of FC-72 on plane cooper are plotted in Fig. 14 [34]. It shows a similar tendency on the transition of the different boiling stages but a little difference in heat flux and corresponding surface temperature. The measured transition from coalescence nucleate boiling to CHF is much more abrupt than the reference curve. That is because of the different conditions of the surface roughness, material, and inclination of the heat source.

While the bubble formation and transit process are dependent on the properties of the liquid coolant, the optimal working condition of the pulse generator with different coolants needs to be further determined experimentally. The heat flux curves of different cooling methods are compared and shown in Fig. 15. With Novec 7200, the avalanche transistor pulse generator obtained the widest frequency variation working area ranging from 20 to 300 kHz, and the maximum temperature can be effectively controlled at around 83 °C, slightly higher than the Novec 7200 boiling temperature T_b 76 °C. The approximately linear heat flux curves of Novec 7500 and Novec 7300 indicate that it only consists of natural convection and discrete bubble boiling stage. This is because the Novec 7300 and the Novec 7500 have a relatively high boiling temperature, making the heat flux needed to reach the full nuclear boiling stage too high for avalanche transistors. The advantage of the phase change cooling was not fully utilized for these coolants. The saturation boiling curves of FC-72, Novec 7100, and Novec 7200 flip over at a temperature of less than 30 °C. At higher temperature, the nucleate boiling heat fluxes for FC-72 becomes slightly higher than Novec 7100, while much higher than Novec 7200. While the temperature further increased, the active nucleation sites density increases (as shown in Fig. 13), lateral coalescence of the growing bubbles decrease the departure frequency, decreasing the difference between the maximum nucleate boiling heat fluxes of FC-72 and Novec 7100. Compared with FC-72 and Novec 7100, Novec 7200 is a better choice for high repetition rate application avalanche transistor pulse generators. The maximum repetition rate as high as 300

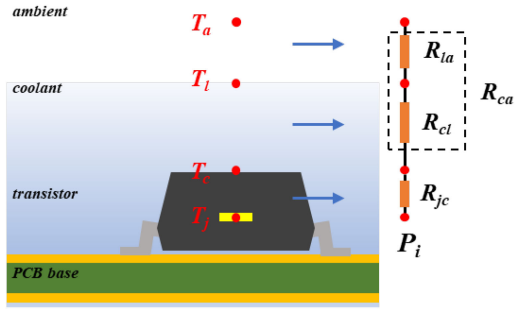

Fig. 16. Schematic of the equivalent heat resistance model.

kHz can be achieved within the allowable temperature range for operation. The measured heat flux at maximum nucleate boiling heat transfer point can provide the guidelines for the thermal design of TPIC with different dielectric fluids.

B. Estimation of the Heat Resistance Under Different Cooling Method

Fig. 16 shows the thermal resistances model of the avalanche transistor in the heat path from junction to ambient. The total thermal resistance between avalanche transistor to the ambient $R_{\theta ja}$ consists of the thermal resistance between junction to the case $R_{\theta jc}$ and $R_{\theta ca}$ that between the case and ambient which includes transistor top side case and coolant $R_{\theta cl}$ and the thermal resistance between coolant to the ambient $R_{\theta la}$, expressed as

$$R_{\theta \mathrm{ja}} = R_{\theta \mathrm{jc}} + R_{\theta \mathrm{ca}} \tag{15}$$

$$R_{\theta \mathrm{ca}} = \frac{T_\mathrm{c} - T_\mathrm{a}}{P} \tag{16}$$

$$T_\mathrm{c} = T_\mathrm{j} - R_{\theta \mathrm{jc}} \times P \tag{17}$$

where T_j, T_c, and T_a represents the junction temperature, case temperature, and ambient temperature, respectively.

The junction temperature must be kept below its maximum rated value by the manufacturer, typically between 125 and 175 °C for Silicon power devices. Based on the datasheet, the safe operating temperature of the avalanche transistor is generally below 150 °C. Due to the existence of the package case, it is impractical to measure the junction temperature directly. We found that thermal destruction always occurred during the experiment when the case temperature was higher than 95 °C. Thus, we can approximately estimate the thermal resistance of the avalanche transistor with FAC, as shown in (16) and (17)

$$R_{\theta \mathrm{jc}}{}^{FAC} = \frac{T_\mathrm{j} - T_\mathrm{c}{}^{FAC}}{P_\mathrm{max}} \approx \frac{150^0\mathrm{C} - 95^0\mathrm{C}}{250\mathrm{mW}} = 220(^\circ\mathrm{C}/W) \tag{18}$$

$$R_{\theta \mathrm{ca}}^{FAC} = R_{\theta \mathrm{ja}}^{FAC} - R_{\theta \mathrm{jc}}^{FAC} \approx 291(^\circ\mathrm{C/W}) \tag{19}$$

where $T_\mathrm{c}{}^{\mathrm{FAC}}$ is the top case temperature at a maximum allowable repetition rate of 80 kHz under FAC. It shows that the thermal resistance between the case and ambient is higher than that between junction to case. According to Mohamed *et al.* [23], the external thermal resistance is about two/third of the total thermal resistance in transistors with the SOT-23 package. It

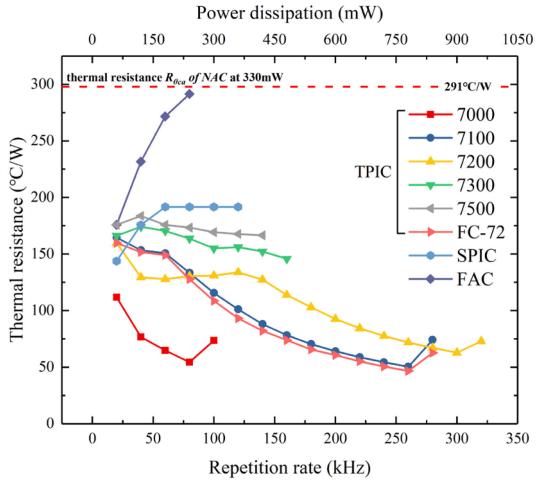

Fig. 17. Comparison of calculated thermal resistance $R_{\theta ca}$ of FAC, SPIC, and TPIC under different power dissipation.

implies that the external resistance $R_{\theta\, ca}$ is the determining factor in the thermal behavior of the avalanche transistors. Based on the measured temperature, the thermal resistance between the case and ambient $R_{\theta\, ca}$ with different cooling techniques is plotted against the repetition rate and power dissipation in Fig. 17.

As shown in Fig. 17, the thermal resistance under different cooling methods shows obvious differences. With operating frequency increases, the thermal resistance $R_{\theta ca}{}^{FAC}$ continues increasing from 175.72 to 291.53 °C/W. Under the high heat flux condition, the FAC technique is incapable of transferring the heat from the transistor surface effectively.

The thermal resistance $R_{\theta ca}{}^{SPIC}$ is much lower than the $R_{\theta ca}{}^{FAC}$. With the repetition rate increases from 20 to 60 kHz, the $R_{\theta ca}{}^{SPIC}$ increases from 143.77 to 191.69 °C/W. As the oil temperature increases, the viscosity and density decrease. It strengthens the natural convection in the liquid, and the thermal resistance remains almost unchanged. However, SPIC is still difficult to meet the heat dissipation requirements under high heat flux density. The maximum repetition rate is limited to 100 kHz.

Compared with the FAC and SPIC techniques, the thermal tendency of TPIC shows a different tendency with the increasing frequency and power dissipation. For FC-72, the equivalent thermal resistance $R_{\theta ca}{}^{FC\text{-}72}$ slightly reduced from 159.74 to 149.09 °C/W with the power dissipation ranged between 60 and 188 mW. Then it decreased from 149.09 to 62.75 °C/W contributing to the phase change of the coolant. These "negative thermal resistance" characteristics of the $R_{\theta ca}{}^{TPIC}$ are of great significance for controlling the temperature rise of devices under high heat flux density. Among the several dielectric liquids, the Novec 7000 has the lowest thermal resistance, while the relatively low boiling temperature limits the further increase of heat flux.

In addition, it is worth noting that the inner pressure of the vessel will increase due to the coolant vaporization, which leads to a higher thermal resistance $R_{\theta ca}{}^{TPIC}$. The increased pressure could drive the boiling point of the coolant up, and it reduces the heat transfer efficiency in the nucleate boiling state. It is not favorable for heat transfer. Therefore, the effective condensation of the vapor inside the vessel is important. While the coolant condensation depends on the temperature difference between the vapor and vessel wall, it could be limited when the temperature of the vessel is close to the boiling point of the coolant. In order to avoid the overheat of the vessel, the operation time of the pulse generator was no longer than 180 s, and a fan cooled the aluminum vessel in the experiment. However, the inner pressure of the vessel has not been obtained since the limitation of the pressure measurement device. While according to the temperature curves, the steady temperature of the avalanche transistor is almost constant at the nucleate boiling stage. Moreover, the voltage waveform shows no change. It indicates that the increase of the inner pressure has little influence on the output parameters in the experiment. The pressure changes inside the vessel in the TPIC and their influence on the thermal resistance are needed further investigation.

Based on the experiment results, we can see that the two-phase immersion cooling technique has the advantage in heat management of the avalanche transistors-based pulse generator. With the TPIC technique, the temperature rise can be effectively controlled, and a more even temperature distribution can be achieved. The thermal resistance between the avalanche transistor case and ambient can be reduced by nearly five times compared with the FAC technique. Moreover, the maximum allowable operation rate of the pulse generator has been improved significantly from 80 to 250 kHz. Accordingly, the experiments showed that the avalanche transistor rating power increases from 330 to 876 mW when a two-phase change cooling technique is used.

C. *Limitation of the TPIC*

Generally, the application of two-phase immersion cooling on the high voltage avalanche transistor pulse generator achieves significant advantages when compared to the FAC and single-phase cooling: much higher allowable repetition rate, higher heat transfer efficiency, and output stability. At the same time, additional considerations should be taken into account. One of the disadvantages when utilizing TPIC is the complexity of the two-phase system. More effective condensers and recycling systems are required for the generators to ensure efficient cooling and avoid the CHF. It will result in expensive and bulky systems. In addition, the cost of the dielectric liquid is much higher than the oil used in SPIC, which could be unbearable for the pulse generator that the huge coolant vessel and a large amount of coolant are needed. Hydrofluorocarbon and perfluorocarbon systems are prone to leakage and resultant global warming emissions. Special attention should be paid to storage, transferring, and recycling. Moreover, the dielectric liquid with a low GWP value, low dielectric constant, and proper boiling temperature for the TPIC technique should be further investigated.

VI. Conclusion

In high power and high repetition avalanche transistors-based pulse generator systems, thermal management could significantly impact the overall performance. Due to the small package

of the components, high heat flux density, inhomogeneous temperature distribution, and fast transient heating process of the pulse circuit, it is of great challenge to develop a compatible and effective cooling system. Therefore, in this article, a TPIC technique with dielectric liquids is applied to a typical avalanche transistor pulse generator, and great improvement of output performance including time-base jitter, voltage amplitude jitter, and maximum repetition rate has been achieved.

1) A simplified calculation model has been developed for the estimation of power dissipation under different frequencies. The calculated maximum repetition rate is less than 100 kHz without the cooling system applied, which fits well with the experimental results ($f_{\max} = 80$ kHz). The increasing ambient temperature will induce the derating of rated power dissipation of the avalanche transistor, and the heat accumulation finally leads to thermal destruction.
2) Forced air convection, single-phase immersion with mineral oil, and two-phase change immersion are applied to the pulse circuits and thoroughly compared. The experiments demonstrate that for the TPIC system, the maximum transistor top surface temperatures are kept below the temperature obtained in FAC, SPIC cooled system under the same operating conditions. It offers the possibility to operate the pulse generator at a higher repetition rate.
3) TPIC shows an advantage in controlling the steady temperature, reducing the time base jitter and voltage amplitude jitter. It can also provide a more even temperature distribution. With TPIC applied (FC-72), the maximum repetition rate is extended to 260 kHz, compared with the FAC of 80 kHz, TPIC of 100 kHz. Under the repetition rate of 80 kHz, the time base jitter can be reduced by 72% compared with FAC.
4) Several dielectric fluids with different properties have been tested with the pulse generator, including 3M Novec 7000, Novec 7100, Novec 7200, Novec 7300, Novec 7500, and FC-72. The Novec 7200 has superiority in the maximum frequency, which could reach 300 kHz at a steady temperature of 84 °C. The dielectric fluids with lower boiling temperatures have the advantage of reducing time-base jitter and voltage amplitude jitter. Due to the dielectric loss, the output amplitude is lower when TPIC is applied. The FC-72 is selected and tested for its balanced performance. The pulse generator with the TPIC technique could achieve output parameters with a peak voltage of 2350 V, a rise time of 180 ps, and the FWHM of 530 ps. It can work stably at 200 kHz for more than 30 min.
5) The desirable operating point of the TPIC is near the end of the fully nucleate boiling region, where the maximum nucleate boiling heat transfer h_{mnq} occurs. The thermal resistance between the transistor case and ambient under different conditions is calculated. The results show that the TPIC can significantly reduce the thermal resistance under a high repetition rate and increase avalanche transistor rating power from 330 to 876 mW. The two-phase change cooling technique offers an attractive solution for the design of high-voltage and high-frequency avalanche transistorized circuits and the other high-voltage repetitive solid-state pulsed power systems.

REFERENCES

[1] J. Jethwa, E. E. Marinero, and A. Muller, "Nanosecond risetime avalanche transistor-circuit for triggering a nitrogen laser," *Rev. Sci. Instrum.*, vol. 52, no. 7, pp. 989–991, 1981.

[2] Y. Mi, Y. Chu, C. Yao, and C. Li, "Development of nanosecond pulsed electric field generator for biological solution treated based on microstrip transmission line," *High Voltage Eng.*, vol. 40, no. 12, pp. 3773–3779, 2014.

[3] I. Adamovich *et al.*, "The 2017 plasma roadmap: Low temperature plasma science and technology," *J. Phys. D-Appl. Phys.*, vol. 50, no. 32, pp. 1–47, Aug. 2017.

[4] I. Y. Immoreev and S. V. Samkov, "Ultra-wideband radar for remote detection and measurement of parameters of the moving objects on small range," in *Proc. 2nd Int. Workshop Ultrawideband Ultrashort Impulse Signals*, 2004, pp. 214–216.

[5] J. Yan, S. Shen, and W. Ding, "High-power nanosecond pulse generators with improved reliability by adopting auxiliary triggering topology," *IEEE Trans. Power Electron.*, vol. 35, no. 2, pp. 1353–1364, Feb. 2020.

[6] W. Ding, Y. Wang, C. Fan, Y. Gou, Z. Xu, and L. Yang, "A subnanosecond jitter trigger generator utilizing trigatron switch and avalanche transistor circuit," *IEEE Trans. Plasma Sci.*, vol. 43, no. 4, pp. 1054–1062, Apr. 2015.

[7] S. Shen, J. Yan, Y. Wang, G. Sun, and W. Ding, "Further investigations on a modified avalanche transistor-based marx bank circuit," *IEEE Trans. Instrum. Meas.*, vol. 69, no. 10, pp. 8506–8513, May 2020.

[8] B. Liang, X. Chen, C. Zhu, and N. Yuan, "Design of high power nanosecond pulsers in UWB radar test system," *J. Microw.*, vol. 37, no. 1, pp. 28–32, 2005.

[9] J. Li *et al.*, "A hybrid pulse combining topology utilizing the combination of modularized avalanche transistor marx circuits, direct pulse adding, and transmission line transformer," *Rev. Sci. Instrum.*, vol. 88, no. 3, 2017, Art. no. 033507.

[10] C. Li, E. Wang, C. Yao, Y. Mi, J. Tan, and R. Zhang, "Compact solid-state Marx-bank sub-nanosecond pulse generator based on gradient transmission line theory," *IEEE Trans. Dielect. Elect. Insul.*, vol. 24, no. 4, pp. 2181–2188, Aug. 2017.

[11] M. Gao *et al.*, "A portable ultrawideband electromagnetic radiator with a 1.4 MW/50 kHz solid-state subnanosecond pulser," *Rev. Sci. Instrum.*, vol. 90, no. 6, Jun. 2019, Art. no. 066102.

[12] Z. Zhao. J. Li, X. Zhong, H. Cao, and M. Zheng, "Design of repetitive nanosecond pulse generator based on modularized marx circuit and transmission line transformer," *Trans. China Electrotech. Soc.*, vol. 32, pp. 121–128, 2017.

[13] Z. Deng, Q. Yuan, S. Shen, J. Yan, Y. Wang, and W. Ding, "High voltage nanosecond pulse generator based on avalanche transistor marx bank circuit and linear transformer driver," *Rev. Sci. Instrum.*, vol. 92, no. 3, 2021, Art. no. 034715.

[14] M. Gao *et al.*, "Traveling-wave Marx circuit for generating repetitive sub-nanosecond pulses," *IEEE Trans. Electromagn. Compat.*, vol. 61, no. 4, pp. 1271–1279, Aug. 2019.

[15] C. S. Sharma, S. Zimmermann, M. K. Tiwari, B. Michel, and D. Poulikakos, "Optimal thermal operation of liquid-cooled electronic chips," *Int. J. Heat Mass Transfer*, vol. 55, no. 7–8, pp. 1957–1969, 2012.

[16] E. Baker, "Liquid immersion cooling of small electronic devices," *Microelectron. Rel.*, vol. 12, no. 2, pp. 163–173, 1973.

[17] W. Jiang, "Repetition rate pulsed power technology and its applications:(vii) Major challenges and future trends," *High Power Laser Part Beams*, vol. 27, no. 1, 2015, Art. no. 010201.

[18] W. Jiang, "Repetition rate pulsed power technology and its applications: (iv) Advantage and limitation of semiconductor switches," *High Power Laser Part Beams*, vol. 25, no. 3, pp. 537–543, 2013.

[19] G. Duan, S. N. Vainshtein, and J. T. Kostamovaara, "Modified high-power nanosecond marx generator prevents destructive current filamentation," *IEEE Trans. Power Electron.*, vol. 32, no. 10, pp. 7845–7850, Oct. 2017.

[20] FMMT 417 datasheet, Diodes Incorporated, Plano, TX, USA, 2010.

[21] X. C. Tong, *Advanced Materials for Thermal Management of Electronic Packaging*. New York, NY, USA: Springer, 2011.

[22] E. Laloya, O. Lucia, H. Sarnago, and J. M. Burdio, "Heat management in power converters: From state of the art to future ultrahigh efficiency systems," *IEEE Trans. Power Electron.*, vol. 31, no. 11, pp. 7896–7908, Nov. 2016.

[23] M. Alli, M. Mahalingam and J. A. Andrews, "Thermal characteristics of plastic small outline transistor (SOT) packages," *IEEE Trans. Compon., Hybrids Manuf. Technol.*, vol. 9, no. 4, pp. 353–363, Dec. 1986.
[24] S. N. Vainshtein, G. Duan, A. V. Filimonov, and J. T. Kostamovaara, "Switching mechanisms triggered by a collector voltage ramp in avalanche transistors with short-connected base and emitter," *IEEE Trans. Electron Devices*, vol. 63, no. 8, pp. 3044–3048, Aug. 2016.
[25] Y. Qiu *et al.*, "High power and high pulse repetition frequency transistorized pulser by time base stability improvement and power synthesis technique," *Rev Sci Instrum.*, vol. 91, no. 8, Aug. 2020, Art. no. 084703.
[26] Heat transfer applications using 3M$^{\mathrm{TM}}$ novec$^{\mathrm{TM}}$, 3M. Company, Saint Paul, MN, USA, 2018.
[27] C. M. Barnes and P. E. Tuma, "Practical considerations relating to immersion cooling of power electronics in traction systems," *IEEE Trans. Power Electron.*, vol. 25, no. 9, pp. 2478–2485, Sep. 2010.
[28] I. Aranzabal, I. M. de Alegria, N. Delmonte, P. Cova, and I. Kortabarria, "Comparison of the heat transfer capabilities of conventional single- and two-phase cooling systems for an electric vehicle IGBT power module," *IEEE Trans. Power Electron.*, vol. 34, no. 5, pp. 4185–4194, May 2019.
[29] A. Bar-Cohen, M. Arik, and M. Ohadi, "Direct liquid cooling of high flux micro and nano electronic components," *Proc. IEEE*, vol. 94, no. 8, pp. 1549–1570, Aug. 2006.
[30] J. Li *et al.*, "Theoretical analysis and experimental study on an avalanche transistor-based marx generator," *IEEE Trans. Plasma Sci.*, vol. 43, no. 10, pp. 3399–3405, Oct. 2015.
[31] G. Duan, S. N. Vainshtein, and J. T. Kostamovaara, "Lateral current confinement determines silicon avalanche transistor operation in short-pulsing mode," *IEEE Trans. Electron Devices*, vol. 55, no. 5, pp. 1229–1236, May 2008.
[32] M. Fernandez, X. Perpina, M. Vellvehi, O. Avino-Salvado, S. Llorente, and X. Jorda, "Power losses and current distribution studies by infrared thermal imaging in soft- and hard-switched IGBTs under resonant load," *IEEE Trans. Power Electron.*, vol. 35, no. 5, pp. 5221–5237, May 2020.
[33] H. Z. Xuelin Yuan *et al.*, "Research on high repetition and high stability pulser based on avalanche transistor," *High Power Laser Part Beams*, vol. 30, no. 1, pp. 64–68, 2010.
[34] P. Krishnaswamy, A. Kuthi, T. Vernier, and M. Gundersen, "Compact subnanosecond pulse generator using avalanche transistors," in *Proc. IEEE 34th Int. Conf. Plasma Sci.*, 2007, pp. 367–367, doi: 10.1109/PPPS.2007.4345673.
[35] H. Z. Xuelin Yuan, Y. Bai, and Z. Ding, "4 kV/30kHz short pulse generator based on time-domain power combining," in *Proc. IEEE Int. Conf. Ultra-Wideband*, 2010, pp. 1–4.
[36] Y. Zhang, B. Liang, J. He, F. Zhang, Y. Zhang, and Y. Zhao, "Design and modified marx nanosecond pulser with high-repetition frequency and high stability" *Res. Prog. Solid State Electron.*, vol. 37, no. 1, pp. 32–35, Feb. 2017.
[37] M. S. El-Genk and J. L. Parker, "Nucleate boiling of FC-72 and HFE 7100 on porous graphite at different orientations and liquid subcooling," *Energy Convers. Manage.*, vol. 49, no. 4, pp. 733–750, 2008.

Yanan Wang (Member, IEEE) received the B.S. and Ph.D. degrees in electrical engineering from Xi'an Jiaotong University, Xi'an, China, in 2014 and 2019, respectively.

He is currently an Assistant Professor with Xi'an Jiaotong University. His current research interests include pulsed power technology, discharge plasma technology, and its application.

Linyuan Ren received the B.S. degree, in 2019, in electrical engineering from Xi'an Jiaotong University, Xi'an, China, where he is currently working toward the Ph.D. degree.

His current research interests include pulsed power technology and electric propulsion.

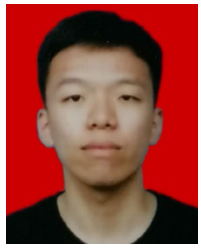

Zihao Yang received the B.S. degree in electrical engineering from Northeast Electric Power University, Jilin City, China, in 2019. He is currently working toward the master's degree with Xi'an Jiaotong University, Xi'an, China.

His current research interests include pulsed power technology.

Zichen Deng received the B.S. degree, in 2020, in electrical engineering from Xi'an Jiaotong University, Xi'an, China, where he is currently working toward the master's degree.

His current research interests include pulsed power technology.

Weidong Ding (Member, IEEE) received the B.S. and M.S. degrees from Xi'an Jiaotong University, Xi'an, China, in 1997 and 2000, respectively, and the Ph.D. degree from Kyushu University, Fukuoka, Japan, in 2007.

He is currently a Professor with Xi'an Jiaotong University. His current research interests include gas discharge, pulsed power technology, and high-voltage measurement.